Chapter 5

Concluding Remarks

5.1 Solar Near-Surface Flows

Supergranulation has wavelike properties. The spectrum of the horizontal divergence of the supergranular flows is consistent with a spectrum of traveling waves with a dispersion relation $\nu \simeq 1.65(l/100)^{0.45}$ μHz. The distribution of wave power is anisotropic with increased power in the direction of rotation and toward the equator, explaining the anomalous motion of the pattern measured by correlation tracking (e.g. super-rotation, see Fig 5.1). The spectrum of supergranulation is Doppler shifted by flows and can be used as a diagnostic tool to probe rotation and meridional circulation in the upper layers of the convection zone. We have shown that the rotation of the plasma through which the pattern propagates is consistent with the rotation of the magnetic network. It is important to note that the main conclusions presented here (Gizon et al., 2003) have recently been confirmed by Schou (2003) with direct Doppler data. Realistic numerical modeling is required to understand supergranulation. Unfortunately the solar convection zone is so highly turbulent and stratified that modeling of the supergranular scales has remained elusive — the most promising calculations are due to DeRosa (2001) and Rieutord et al. (2001).

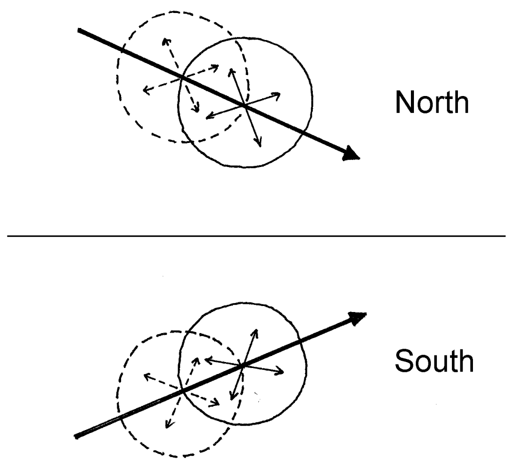

Figure 5.1: Propagation of the supergranules with respect to the local flow. After about 3 days the divergence pattern (solid) is anti-correlated with the initial pattern (dashed). The direction of propagation is prograde and toward the equator in both hemispheres.

Supergranular flows have a net kinetic helicity. We showed that the vertical vorticity of the supergranular flows (curl) is anti-correlated with the horizontal divergence (div) in the northern hemisphere, and that the latitudinal variation of $\langle \mathrm{div}\,\mathrm{curl} \rangle$ can be explained by the effect of the Coriolis force on convection (Gizon & Duvall, 2003). Parker (1955) proposed that the magnetic field can grow in a moving medium with a net kinetic helicity, $\mathcal{H}_{\mathrm{kin}} = \langle \boldsymbol{v} \cdot \boldsymbol{\nabla} \times \boldsymbol{v} \rangle \neq 0$. Cyclonic convection is also invoked as an important mechanism for generating a large-scale poloidal field from an initial toroidal field. Although we only observe the two horizontal components of velocity, we may use a proxy for the average kinetic helicity (Rüdiger et al., 1999): $\mathcal{H}_{\mathrm{kin}} \sim H_{\mathrm{m}} \, \langle \mathrm{div}\,\mathrm{curl} \rangle$, where $H_{\mathrm{m}} = -\langle \partial_z \ln|\rho v_z| \rangle^{-1}$ is the average vertical momentum scale height, expected to be positive. Hence, our measurements would suggest a negative kinetic helicity in the north for supergranulation. However, turbulence may also be driven by magnetic buoyancy (Brandenburg & Schmitt, 1998; Rüdiger et al., 2001) and it may be of interest to search for solar cycle variations in the quantity $\langle \mathrm{div}\,\mathrm{curl} \rangle$. Our observations give hope for a direct measurement of the kinetic helicity in the upper convection zone that would perhaps constrain models of the solar dynamo.

Local flows associated with magnetic active regions. Yoshimura (1971) suggested a long time ago that the longitudinal ordering of solar magnetic fields may be explained by the existence of large convective patterns. Earlier attempts at detecting such flows in direct Doppler data proved difficult (e.g. Scherrer et al., 1986). The observations presented in section 2.4 provide reliable evidence for extended surface flows converging toward active regions with an amplitude of 50 m/s at most (Gizon et al., 2001b, , see Fig. 5.2). The time-distance results agree with the ring analysis (Hindman et al., 2003) and are consistent with claims by Howard (1996) that plages drift toward the mean latitude of activity. Perhaps the observed flows favor the formation of active regions at particular sites on the solar surface; but these flows may also be a secondary consequence of the emergence of the magnetic flux. On a larger scale, Beck et al. (1998) and Ulrich (2001) have found evidence for long-lived giant velocity patterns, with no obvious connection to patterns of magnetic activity.

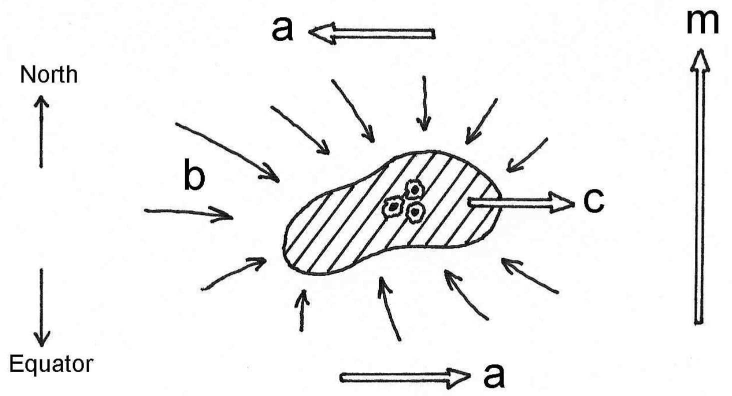

Figure 5.2: Sketch of horizontal flows around an active region, measured 1 Mm below the surface with time-distance helioseismology. (b) Active regions are surrounded by a $\sim$ 50 m/s converging flow. (a) Zonal flows switch sign near active latitudes (± 5 m/s). (m) Poleward 20 m/s meridional flow. (c) The magnetized plasma rotates a little faster than the quiet Sun.

Solar-cycle variability of the meridional circulation and differential rotation. At the surface the flows associated with complexes of magnetic activity are superimposed on the "torsional oscillations" that migrate equatorward with an eleven year period and an amplitude of the order of 5 m/s. It has been suggested that the "torsional oscillations" may be driven by the Lorentz force due to a migrating dynamo wave (Schüssler, 1981) or caused by a thermal effect due to surface magnetic fields (Spruit, 2003). We have shown that the "torsional oscillations" have both an east-west and a north-south component (Beck et al., 2002). The east-west component of the torsional oscillation shows a shear around the latitude of mean activity with the same sign at the surface and deeper in the convection zone. The p-mode travel times reveal residual flows in the meridional plane that diverge from the mean latitude of activity, tens of megameters below the surface. On the other hand, flows that converge toward the latitude of mean activity are seen near the surface. This suggests the existence of two rolls with helical streamlines of opposite handedness on each side of the latitude of mean activity. Figure 5.3 reviews the observations and displays the proposed flow geometry of the "torsional oscillations".

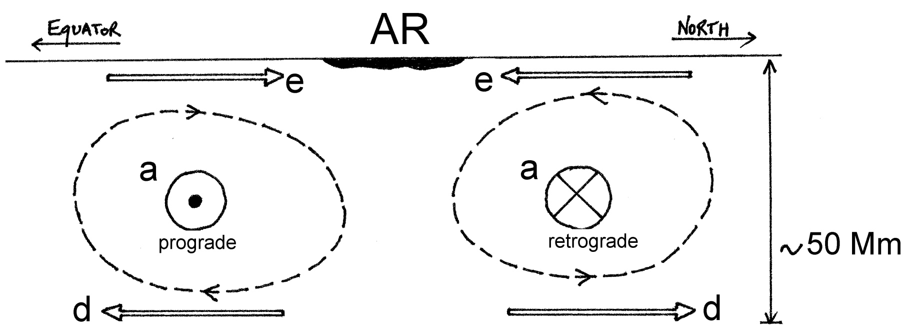

Figure 5.3: Meridional cut in the northern hemisphere showing longitudinal averages of the residual flows (with respect to smooth fits to the rotation and meridional circulation) around the mean latitude of activity (AR). (e) 5 m/s inflow near the surface (f modes). (d) Outflow as deep as 65 Mm below the surface (p modes). (a) ± 5 m/s sheared zonal flow throughout the upper convection zone. Observations are consistent with the existence of two counter-rotating meridional cells centered about the mean latitude of activity (dashed), superimposed on the 20 m/s large-scale meridional circulation.

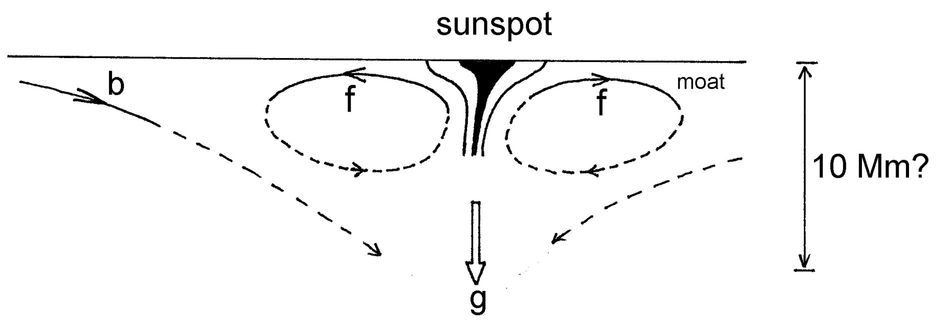

Figure 5.4: Tentative sketch of flows under sunspots. (f) Near-surface horizontal outflow with values up to 1 km/s, called the moat. The horizontal extent of the moat flow is $\sim$ 30 Mm from the center of the sunspot. (b) Well beyond the moat is a large-scale $\sim$ 50 m/s inflow, as shown in Fig. 5.2. (g) Under the sunspot is a $\sim$ 1 km/s downflow (Duvall et al., 1996; Zhao et al., 2001). The dashed lines are proposed model streamlines consistent with (most) observations. The vertical scale is uncertain.

Sunspot flows. As mentioned in the introduction, Gizon et al. (2000) have studied near-surface flows around sunspots. Wave-based sensitivity kernels for horizontal flows were used in an iterative deconvolution of f-mode travel times (high-resolution MDI data). Because these results are still preliminary, we shall only mention that the horizontal outflow around a sunspot, called the moat (e.g. Solanki, 2003), was detected. This outflow was detected earlier by Lindsey et al. (1996), deeper inside the Sun. Figure 5.5 shows a map of the horizontal flows near the surface for one sunspot observed on Dec 6, 1998 (the horizontal spatial resolution is 3 Mm). The internal structure of flows under sunspots is still largely unknown. Duvall et al. (1996) and Zhao et al. (2001) have detected downflows below sunspots and Braun & Lindsey (2003) observe the moat outflow down to a depth of 3 Mm. Fig. 5.4 is an attempt to show how the flows measured with f-mode time-distance helioseismology *may* fit into a consistent picture.

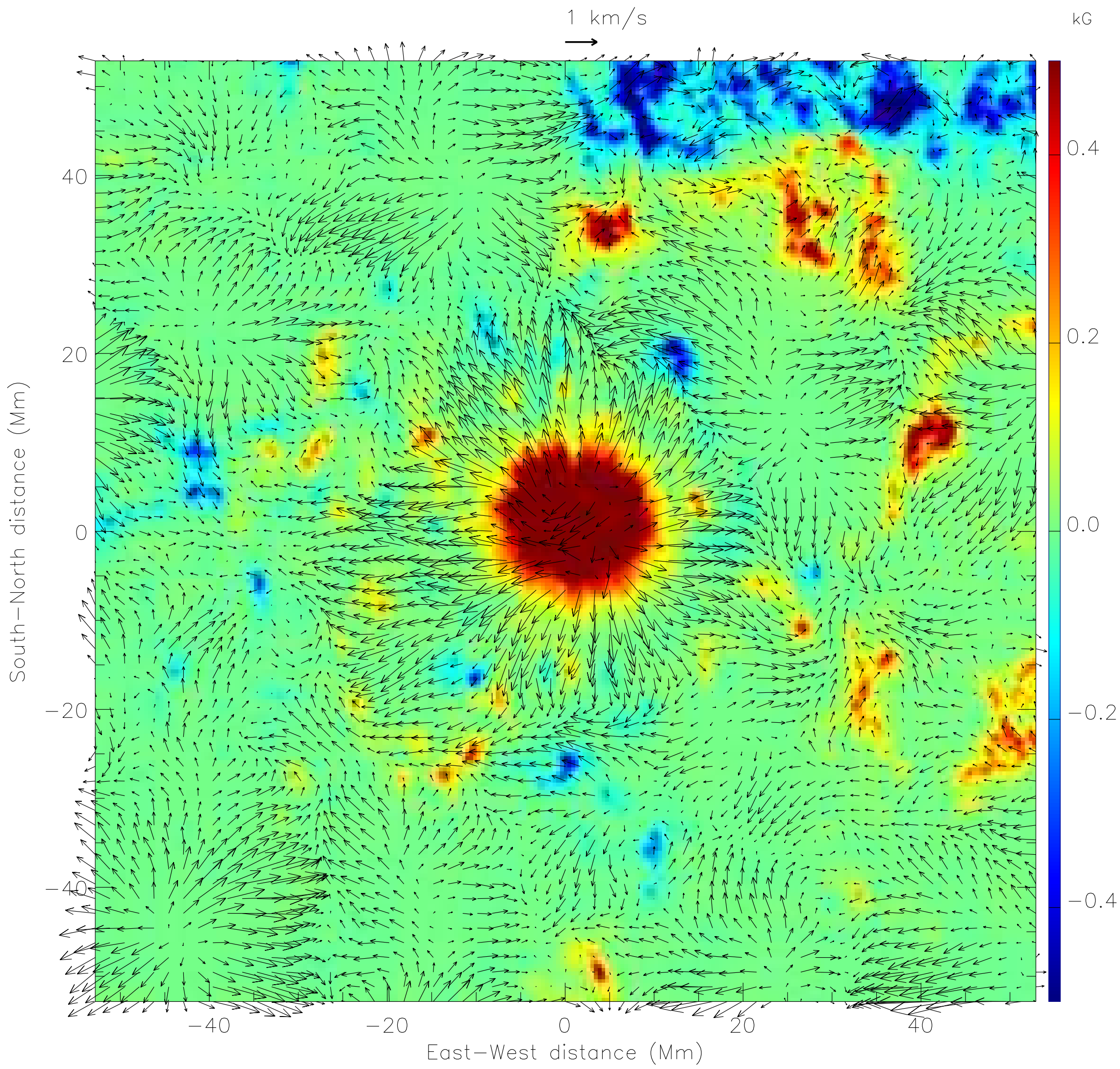

Figure 5.5: Horizontal flows around a sunspot on Dec 6, 1998, obtained with f-mode time-distance helioseismology (Gizon et al., 2000). Overplotted is the line-of-sight magnetic field (MDI high resolution) truncated at ±0.5 kG. The moat flow beyond the penumbra (red) is clearly visible.

5.2 Toward Travel-Time Sensivity Kernels

We now have a general recipe (§ 3.2) for solving the linear forward problem, i.e. computing travel-time sensitivity kernels. This recipe is based on a physical description of the observed wave field. The kernels give the linear dependence of travel-time perturbations on perturbations to a solar model and they take account of the details of the measurement procedure. The sensitivity kernels depend on the background solar model, on the filtering and fitting of the data, and on position on the solar disk (through the line of sight).

In section 3.3 we have shown how to compute the 2D sensitivity of travel-time perturbations to source and damping inhomogeneities for surface gravity waves. This example was important as it shows that kernels can be obtained, using our recipe, once the physics of the model is fully specified. In particular the source spectrum and the details of the observation procedure need to be specified at the start of the problem and appear explicitly in the expression for the travel-time kernels.

The model with random excitation sources reveals some important details in the sensitivity kernels that are not accounted for in the single source model. In particular, the single-source kernels show only ellipse shaped features, while the distributed-source kernels show both hyperbola and ellipse shaped features. Computations of kernels in the single-source picture are as difficult, both analytically and numerically, as kernels in the distributed-source picture.

The example we have presented is a simplified model for the solar f mode. Improvements to the model would include stratification, spherical geometry, compressibility, and a physical model of excitation and damping. In particular, in a compressible medium the effect of the conversion of p modes into f modes by scattering could be computed. Despite these limitations, we believe that our 2D example kernels can be useful in studying solar problems using time-distance helioseismology. The kernels may be interpreted as depth averages over the first few Mm below the photosphere of the three-dimensional solar kernels (Duvall & Gizon, 2000).

Woodard (1997) performed an analysis of the effect of localized damping on travel times for acoustic waves; this analysis showed that for a model sunspot, with radius 10 Mm, the travel-time difference is of order -1 minute, in the case where **1** is located at the center of the sunspot and **2** is a distance 10 Mm away. For the same geometry the kernel $K^{\gamma}_{\rm diff}$, which we have computed, predicts a positive travel-time difference of 1 s for a 50% increase in damping rate. These two apparently conflicting results are, however, for different types of waves and quite different models for the effect of damping inhomogeneities. The damping perturbation employed by Woodard (1997) can be understood in terms of a reduction in source strength for sources located behind the sunspot from the observation points, as scattering by the damping inhomogenetıes was neglected. There remains work to be done on this subject. For example, it is known that absorption by magnetic structures is a strong function of frequency (Braun et al., 1988; Bogdan et al., 1993). This effect could be modeled by writing kernels for local changes to the exponent β in equation (3.57) for the damping rate. We plan to do a quantitative analysis of this problem in the future. Note that perturbations in sunspots are strong and that linear theory may not be accurate in this case (e.g. Cally & Bogdan, 1997)

The most significant obstacle to the computation of accurate travel-time kernels is our lack of a detailed understanding of turbulent convection. The excitation and damping of solar oscillations is due to convection and is thus extremely difficult to account for in the background model: approximations must be introduced. In chapter 3 we employed a phenomenological model based on observed properties of solar convection. An important constraint on the zero-order solar model is that it must produce a k-ω diagram compatible with observations. A further complication introduced by turbulence is that, in principle, it demands a theory for wave propagation through random media, i.e. a treatment of perturbations that vary on short temporal and spatial scales.

We have not addressed the computation of three dimensional travel time kernels in a spherical solar model. Preliminary efforts have shown that such a computation is feasible, but is demanding (Birch & Kosovichev, 2000). There are a number of less fundamental issues relating to the interpretation of travel times. We emphasize that the filter $\mathcal{F}$ includes the point spread function of the instrument, which is not always well known. It is unclear how an inaccurate estimate of the point spread function affects the interpretation of travel-time measurements. A straightforward issue is that cross-correlations are typically averaged over annuli or sectors of annuli

(Duvall et al., 1997); this can easily be accounted for by averaging the point-to-point kernels described in chapter 3.

The inverse problem, using measured travel times to learn about how the Sun differs from a model, is an entirely separate issue and beyond the scope of this thesis. We wish to note, however, that techniques for the 3D inversion of time-distance data have already been developed (Kosovichev, 1996; Jensen et al., 1998). The errors in the travel-time measurements, which are essential to solving the inverse problem, are mainly due to realization noise. The formalism presented in this thesis will be helpful in estimating these errors.

5.3 Prospects for Asteroseismology

We have shown that the inclination angle, i, of the axis of rotation of a Sun-like star can in principle be determined with great precision using the techniques of asteroseismology. The observational requirement is a long nearly-continuous time series sampled at a high cadence. The missions COROT and Eddington will provide such data for a large number of stars, with continuous observation for up to 5 and 36 months, respectively. The Danish project MONS (Kjeldsen & Bedding, 1998) aims at targeting individual stars for up to 2 months with a high duty cycle. We have found that it is difficult to estimate the inclination angle for stars with $i < 30°$, whereby this limit is lower for more rapidly rotating stars. Note however that, statistically, more than 85% of the stars have $i > 30°$.

Gough et al. (1995) applied essentially the same method to estimate the inclination angle of the Sun. Solar p modes were observed continuously in irradiance for 160 days in 1988 by the IPHIR experiment (PHOBOS mission). Gough et al. (1995) found the ratio between the power in $(l = 1, m = 0)$ modes and $(l = 1, m = \pm 1)$ modes to be less then 0.0009, i.e. $i > 89.96°$. They pointed out that at the time of the observations the mean inclination of the rotation axis of the solar surface was $i = 85°$, corresponding to an expected ratio of 0.015. Although this discrepancy could be interpreted as a depth dependence in the direction of the solar rotation axis, it is more likely that it is due to a measurement bias. Examination of Figure 4.4a reveals that the fitting procedure preferentially returns values $i^{\star} \approx 90°$

for inclination angles in the range $80° < i < 90°$. Besides, the hypothesis of solar rotation about a unique axis is consistent with spatially-resolved LOI data (Gizon et al., 1998). From an astronomer's point of view, it should be clear that Gough et al. (1995) were successful in measuring i with a good precision. We also note that Paunzen et al. (1998) used a somewhat similar diagnostic, i.e. the amplitude ratio of $m = \pm 1$ and $m = 0$ dipole gravity modes, to estimate the inclination of an oscillating pre-white dwarf star (although their formulas appear to be incorrect).

The precision that can be achieved on the measurement of i depends on each individual star. First of all, acoustic modes must be excited to a sufficiently high amplitude. In Sect 4.1 we fixed luminosity amplitudes at their solar value with respect to the background noise. Houdek et al. (1999) presented estimates of oscillation amplitudes in main-sequence stars derived from model calculations of stellar convection. They found that velocity amplitudes essentially scale like the mass-to-light ratio of the star, in agreement with an earlier prediction by Kjeldsen & Bedding (1995). The noise background may also vary. Here we took $S/N = 100$, but it has been shown that a useful estimate of i can be obtained when the signal-to-noise ratio is as low as $S/N = 20$ (Gizon, 2002).

Another condition for determining i is a sufficiently large stellar rotation rate, in order to resolve azimuthal modes split by rotation. This condition is met when the angular velocity of the star, Ω, is at least twice larger than the linewidth, Γ, of the modes of oscillation. Since Γ is a decreasing function of frequency, the analysis of low-frequency multiplets may be crucial in order to measure the inclination angle of slowly rotating stars. We refer the reader to the work of Houdek et al. (1999) for a study of the variation of mode damping with frequency and stellar parameters.

A single realization of the power spectrum will be available for a particular star. How will we know when a measurement of i is meaningful? A large set of Monte-Carlo simulations will be essential in assessing the reliability of a measurement. As we saw in this study, the answer is likely to be very reliable for several outcomes of the minimization procedure (e.g. large $\Omega^\star$ and large $i^\star$). In general the fit also returns an error bar on each estimated parameter which could be used to further increase the confidence in a measurement. Finally we repeat that the precision on i can be improved by considering more than one multiplet in the power spectrum. As a rough estimate, the error on i goes like $n^{-1/2}$, where n is the number of multiplets. The exact number of potentially usable modes depends on the oscillation amplitudes for a particular star. For the Sun, tens of modes can be employed (Fig. 4.1).

The technique that we have described also provides accurate measurements of the angular velocity, Ω (Fig. 4.9). For active Sun-like stars Ω may also be determined by following surface tracers (photometry). By comparing the Ω determined from oscillations with the angular velocity from tracers, inferences can be made on the stellar differential rotation. A knowledge of this quantity, particularly for more rapidly rotating stars, would be of great interest (e.g., for dynamo theories). Alternatively, for those stars for which accurate astrometrically determined parallaxes are known and from which radii $R_\star$ have been determined, a comparison of $\Omega R_\star \sin i$ obtained from asteroseismology with $v \sin i$ determined spectroscopically could set limits on the differential rotation. Differential rotation could also be determined seismically by measuring the rotational splitting frequencies of the quadrupole modes with $m = \pm 1$ and $m = \pm 2$ (when i is such that these modes are visible).

Appendix A

Definition of Travel Time

According to equation (3.5) the travel times $\tau_+(\mathbf{1},\mathbf{2})$ and $\tau_-(\mathbf{1},\mathbf{2})$ are the time lags which minimize the functions

$$X_\pm(\mathbf{1},\mathbf{2},t) = \int_{-\infty}^{\infty} \mathrm{d}t'\ f(\pm t')\left[C(\mathbf{1},\mathbf{2},t') - C^{\mathrm{ref}}(\mathbf{1},\mathbf{2},t' \mp t)\right]^2 . \tag{A.1}$$

As a result the time derivatives of $X_\pm$ evaluated at $\tau_\pm$ are zero:

$$\dot{X}_\pm(\mathbf{1},\mathbf{2},\tau_\pm) = 0 . \tag{A.2}$$

Notice that $\dot{X}$ does not involve a time derivative of the observed cross-correlation C. In order to obtain the travel-time perturbations $\delta\tau_\pm$ we need to linearize around the zero-order travel times $\tau^0_\pm$, which are defined by

$$\tau^0_\pm(\mathbf{1},\mathbf{2}) = \underset{t}{\mathrm{argmin}}\{\ X^0_\pm(\mathbf{1},\mathbf{2},t)\ \} . \tag{A.3}$$

The functions $X^0_\pm$ refer to equation (A.1) evaluated for $C = C^0$, where C^0 is the zero-order cross-correlation in the reference model. Linearizing equation (A.2) about $\tau_\pm = \tau^0_\pm$ gives

$$\delta\tau_\pm(\mathbf{1},\mathbf{2}) = -\frac{\delta\dot{X}_\pm(\mathbf{1},\mathbf{2},\tau^0_\pm)}{\ddot{X}^0_\pm(\mathbf{1},\mathbf{2},\tau^0_\pm)} . \tag{A.4}$$

The functions $\delta\dot{X}_\pm$ are given by

$$\delta\dot{X}_\pm(\mathbf{1},\mathbf{2},t) = \pm 2\int_{-\infty}^{\infty} \mathrm{d}t'\ f(\pm t')\dot{C}^{\mathrm{ref}}(\mathbf{1},\mathbf{2},t'\mp t)\delta C(\mathbf{1},\mathbf{2},t')\,. \tag{A.5}$$

We can then compute $\ddot{X}^0(\tau^0_\pm)$ by straigtforward differentiation of equation (A.1). The result for $\delta\tau_\pm(\mathbf{1},\mathbf{2})$ is thus

$$\delta\tau_\pm(\mathbf{1},\mathbf{2}) = \int_{-\infty}^{\infty} \mathrm{d}t\ W_\pm(\mathbf{1},\mathbf{2},t)\delta C(\mathbf{1},\mathbf{2},t)\,, \tag{A.6}$$

with

$$W_\pm(t) = \frac{\pm f(\pm t)\dot{C}^{\mathrm{ref}}(t\mp\tau^0_\pm)}{\int_{-\infty}^{\infty}\mathrm{d}t'\ \left[f(\pm t')C^0(t')\ddot{C}^{\mathrm{ref}}(t'\mp\tau^0_\pm) \pm \dot{f}(\pm t')C^{\mathrm{ref}}(t'\mp\tau^0_\pm)\dot{C}^{\mathrm{ref}}(t'\mp\tau^0_\pm)\right]}\,. \tag{A.7}$$

We have supressed the spatial arguments **1** and **2** in the above equation for the sake of readability. This is the general linearized result for arbitrary C^{ref} and f. The only assumption is that the perturbation to the cross-correlation is small compared to the zero-order cross-correlation. Note that we have not written an explicit expression for $\tau^0_\pm$, which needs to be computed numerically by minimizing $X^0_\pm(t)$ (eq. [A.3]).

In the case where C^{ref} and C^0 are even in time, $\tau^0_+ = \tau^0_-$. For the choice $C^{\mathrm{ref}} = C^0$, the zero-order travel times are both zero, $\tau^0_\pm = 0$. This choice is recommended if a theoretical model is available to the observer. With $C^{\mathrm{ref}} = C^0$ the weight functions $W_\pm$ simplify to:

$$W_\pm(\mathbf{1},\mathbf{2},t) = \frac{\mp f(\pm t)\dot{C}^0(\mathbf{1},\mathbf{2},t)}{\int_{-\infty}^{\infty}\mathrm{d}t'\ f(\pm t')[\dot{C}^0(\mathbf{1},\mathbf{2},t')]^2}\,. \tag{A.8}$$

In the example presented in Section 3.3 we choose $C^{\mathrm{ref}} = C^0$ and $f(t) = \mathrm{Hea}(t)$.

Appendix B

Fourier Convention

Given a function $q(\boldsymbol{x}, t)$, of horizontal position $\boldsymbol{x}$ and time t, we employ the convention that the function $q(\boldsymbol{x}, t)$ and its Fourier transform $\check{q}(\boldsymbol{k}, \omega)$ are related by

$$q(\boldsymbol{x}, t) = \iint_{-\infty}^{\infty} \mathrm{d}\boldsymbol{k} \int_{-\infty}^{\infty} \mathrm{d}\omega \; e^{\mathrm{i}\boldsymbol{k}\cdot\boldsymbol{x} - \mathrm{i}\omega t} \, \check{q}(\boldsymbol{k}, \omega) \, , \tag{B.1}$$

$$\check{q}(\boldsymbol{k}, \omega) = \frac{1}{(2\pi)^3} \iint_{-\infty}^{\infty} \mathrm{d}\boldsymbol{x} \int_{-\infty}^{\infty} \mathrm{d}t \; e^{-\mathrm{i}\boldsymbol{k}\cdot\boldsymbol{x} + \mathrm{i}\omega t} \, q(\boldsymbol{x}, t) \, , \tag{B.2}$$

where $\boldsymbol{k}$ is a two-dimensional horizontal wave vector and ω is the angular frequency. We commonly use the same symbol for q and $\check{q}$: the arguments make clear whether the function or its transform is intended. We use the notation $q(k, \omega)$ when $q(\boldsymbol{k}, \omega)$ only depends on the magnitude of $\boldsymbol{k}$, not its direction, for example in the filter function $F(k, \omega)$. We note that for functions $q(\boldsymbol{x}, t)$ which do not vanish at large $\|\boldsymbol{x}\|$ or $|t|$ the Fourier transform is not defined. In particular there is a problem for the case when the observable is not windowed in space or time. In such a case, $q(\boldsymbol{k}, \omega)$ is intended to mean the Fourier transform of the function $q(\boldsymbol{x}, t)$ truncated to zero for $|t| > T/2$ and $\|\boldsymbol{x}\| > \sqrt{A/\pi}$, where the time interval T and the area A are both large and finite. This modification enables us to refer to the Fourier transform of a stationary/homogeneous random function (cf. Yaglom, 1962, for a rigorous formalism).

When a function of four arguments, $Q(\boldsymbol{x}, t; \boldsymbol{x}', t')$, depends only on the separations $\boldsymbol{x} - \boldsymbol{x}'$ and $t - t'$ (translation invariance), we use the following conventions:

$$Q(\boldsymbol{x} - \boldsymbol{x}', t - t') = Q(\boldsymbol{x}, t; \boldsymbol{x}', t')\,, \tag{B.3}$$

$$Q(\boldsymbol{k}, \omega) = \frac{1}{(2\pi)^3} \iint_{-\infty}^{\infty} \mathrm{d}\boldsymbol{x} \int_{-\infty}^{\infty} \mathrm{d}t\; e^{-\mathrm{i}\boldsymbol{k}\cdot\boldsymbol{x} + \mathrm{i}\omega t}\, Q(\boldsymbol{x}, t)\,. \tag{B.4}$$

The above conventions are employed, in our example, for the functions $m^0(k, \omega)$, $\boldsymbol{G}(\boldsymbol{k}, \omega; z)$, and $\mathcal{G}(k, \omega)$.

Finally, we recall the relations

$$\int_{-\infty}^{\infty} \mathrm{d}t\; e^{\mathrm{i}\omega t} = 2\pi\, \delta_{\mathrm{D}}(\omega)\,, \tag{B.5}$$

$$\iint_{-\infty}^{\infty} \mathrm{d}\boldsymbol{x}\; e^{-\mathrm{i}\boldsymbol{k}\cdot\boldsymbol{x}} = (2\pi)^2\, \delta_{\mathrm{D}}(\boldsymbol{k})\,, \tag{B.6}$$

which are very useful in rewriting the kernels in Fourier space (Appendix C).

Appendix C

Travel Time Sensitivity Kernels for the Example

In this Appendix we derive surface gravity wave travel time kernels, $K^a_\pm$ and $K^\gamma_\pm$, for perturbations to local source strength and damping rate respectively. These kernels connect travel times perturbations, $\delta\tau_\pm$, to perturbations to the model:

$$\delta\tau_\pm(\mathbf{1},\mathbf{2}) = \int_{(A)} \mathrm{d}\boldsymbol{r}\, \frac{\delta a(\boldsymbol{r})}{a}\, K^a_\pm(\mathbf{1},\mathbf{2};\boldsymbol{r}) + \int_{(A)} \mathrm{d}\boldsymbol{r}\, \frac{\delta\gamma(\boldsymbol{r})}{\gamma}\, K^\gamma_\pm(\mathbf{1},\mathbf{2};\boldsymbol{r})\,. \tag{C.1}$$

Here $\delta a(\boldsymbol{r})/a$ is the local fractional change in the source strength and $\delta\gamma(\boldsymbol{r})/\gamma$ the local fractional change in damping rate. The spatial integral $\int_{(A)} \mathrm{d}\boldsymbol{r}$ is a two-dimensional integral taken over all points $\boldsymbol{r}$ on the surface $z = 0$. From the theory part of this paper (§ 3.2) we know that in order to compute kernels we first need to write the perturbation to the cross-correlation in terms of the functions $\mathcal{C}^a$ and $\mathcal{C}^\gamma$ (see eq. [3.29]):

$$\delta C(\mathbf{1},\mathbf{2},t) = \int_{(A)} \mathrm{d}\boldsymbol{r}\, \frac{\delta a(\boldsymbol{r})}{a}\, \mathcal{C}^a(\mathbf{1},\mathbf{2},t;\boldsymbol{r}) + \int_{(A)} \mathrm{d}\boldsymbol{r}\, \frac{\delta\gamma(\boldsymbol{r})}{\gamma}\, \mathcal{C}^\gamma(\mathbf{1},\mathbf{2},t;\boldsymbol{r})\,. \tag{C.2}$$

The general expression for $\delta C(\mathbf{1},\mathbf{2},t)$ is given by equations (3.25), (3.26), and (3.27). In our example, however, the superscripts on the Green's function can be dropped as the source S is scalar. To obtain $\mathcal{C}^a$, we use equation (3.27) for $\mathcal{C}_S$ and the definition of the source perturbation δM (eqs. [3.49] and [3.53]). After integrations by parts on the source variables in the right-hand side of equation (3.27) and the change of variables $\boldsymbol{r} = (\boldsymbol{s}+\boldsymbol{s}')/2$ and $\boldsymbol{u} = \boldsymbol{s}-\boldsymbol{s}'$, we obtain

$$\begin{aligned}\mathcal{C}^a(\mathbf{1},\mathbf{2},t;\boldsymbol{r}) &= \frac{1}{T}\int \mathrm{d}t'\,\mathrm{d}t_\mathrm{s}\,\mathrm{d}t'_\mathrm{s}\,\mathrm{d}\boldsymbol{u}\; m^0(\boldsymbol{u},t_\mathrm{s}-t'_\mathrm{s}) \\ &\quad\times \mathcal{G}^{\boldsymbol{\Pi}}(\mathbf{1}-\boldsymbol{r}-\boldsymbol{u}/2,t'-t_\mathrm{s})\,\mathcal{G}^{\boldsymbol{\Pi}}(\mathbf{2}-\boldsymbol{r}+\boldsymbol{u}/2,t'-t'_\mathrm{s}+t)\,. \quad (\mathrm{C}.3)\end{aligned}$$

The function $\mathcal{C}^\gamma$ is obtained from equation (3.26) with $\delta\mathcal{L}$ defined by equations (3.46) and (3.58). After integrations by parts on the source variables, and a partial integration on the variable $\boldsymbol{r}$, the result is:

$$\begin{aligned}\mathcal{C}^\gamma(\mathbf{1},\mathbf{2},t;\boldsymbol{r}) &= \frac{1}{2\pi T}\int \mathrm{d}t'\,\mathrm{d}t''\,\mathrm{d}\boldsymbol{s}\,\mathrm{d}t_\mathrm{s}\,\mathrm{d}\boldsymbol{s}'\,\mathrm{d}t'_\mathrm{s}\,\mathrm{d}\bar{t}\;\Gamma^0(t''-\bar{t})\,m^0(\boldsymbol{s}-\boldsymbol{s}',t_\mathrm{s}-t'_\mathrm{s}) \\ &\quad\times \boldsymbol{\nabla}^2_\mathrm{h}\dot{\boldsymbol{G}}_\mathrm{h}(\boldsymbol{r}-\boldsymbol{s},\bar{t}-t_\mathrm{s})\cdot\Big[\mathcal{G}^{\boldsymbol{\Pi}}(\mathbf{1}-\boldsymbol{s}',t'-t'_\mathrm{s})\,\boldsymbol{\nabla}_\mathrm{h}\dot{\mathcal{G}}(\mathbf{2}-\boldsymbol{r},t'+t-t'') \\ &\quad+\mathcal{G}^{\boldsymbol{\Pi}}(\mathbf{2}-\boldsymbol{s}',t'+t-t'_\mathrm{s})\,\boldsymbol{\nabla}_\mathrm{h}\dot{\mathcal{G}}(\mathbf{1}-\boldsymbol{r},t'-t'')\Big]\,, \quad (\mathrm{C}.4)\end{aligned}$$

where $\boldsymbol{G}_\mathrm{h}$ denotes the two horizontal components of the vector $\boldsymbol{G}$. In the space-time domain these integrals are quite complicated to compute. They, however, are greatly simplified when written in terms of the Fourier transforms of the various functions:

$$\begin{aligned}\mathcal{C}^a(\mathbf{1},\mathbf{2},t;\boldsymbol{r}) &= (2\pi)^4\int \mathrm{d}\omega\,\mathrm{d}\boldsymbol{k}\,\mathrm{d}\boldsymbol{k}'\;e^{\mathrm{i}\boldsymbol{k}\cdot\boldsymbol{\Delta}_1-\mathrm{i}\boldsymbol{k}'\cdot\boldsymbol{\Delta}_2-\mathrm{i}\omega t}\,m^{0*}[(\boldsymbol{k}+\boldsymbol{k}')/2,\omega] \\ &\quad\times \mathcal{G}^{\boldsymbol{\Pi}*}(\boldsymbol{k},\omega)\,\mathcal{G}^{\boldsymbol{\Pi}}(\boldsymbol{k}',\omega)\,, \quad (\mathrm{C}.5)\\ \mathcal{C}^\gamma(\mathbf{1},\mathbf{2},t;\boldsymbol{r}) &= (2\pi)^7\int \mathrm{d}\omega\,\mathrm{d}\boldsymbol{k}\,\mathrm{d}\boldsymbol{k}'\;\left(e^{\mathrm{i}\boldsymbol{k}\cdot\boldsymbol{\Delta}_1-\mathrm{i}\boldsymbol{k}'\cdot\boldsymbol{\Delta}_2-\mathrm{i}\omega t}+e^{\mathrm{i}\boldsymbol{k}\cdot\boldsymbol{\Delta}_2-\mathrm{i}\boldsymbol{k}'\cdot\boldsymbol{\Delta}_1+\mathrm{i}\omega t}\right) \\ &\quad\times\Gamma^0(\omega)m^0(\boldsymbol{k},\omega)G^{\Pi}(\boldsymbol{k},\omega)\mathcal{G}^{\boldsymbol{\Pi}*}(\boldsymbol{k},\omega)\;\hat{\boldsymbol{k}}\cdot\hat{\boldsymbol{k}}'\;\mathcal{G}^{\boldsymbol{\Pi}}(\boldsymbol{k}',\omega)/k'\,. \quad (\mathrm{C}.6)\end{aligned}$$

We have used the definitions

$$\begin{aligned}\mathcal{G}^{\boldsymbol{\Pi}}(\boldsymbol{k},\omega) &= F(\boldsymbol{k},\omega)G^{\boldsymbol{\Pi}}(\boldsymbol{k},\omega)\,, \quad (\mathrm{C}.7)\\ G^{\boldsymbol{\Pi}}(\boldsymbol{k},\omega) &= \mathrm{i}\omega k^2 G_z(\boldsymbol{k},\omega;z=0)\,, \quad (\mathrm{C}.8)\end{aligned}$$

and the identity $\boldsymbol{G}_\mathrm{h}(\boldsymbol{k},\omega) = \mathrm{i}\hat{\boldsymbol{k}}G_z(\boldsymbol{k},\omega)$ resulting from equation (3.70). The Green's function $G_z(k,\omega)$ is the $\hat{\boldsymbol{z}}$ component of $\boldsymbol{G}$, given by equation (3.70).

With the assumption that m^0 is independent of $\boldsymbol{k}$, the above expressions can be simplified to

$$\mathcal{C}^{a}(\mathbf{1},\mathbf{2},\omega;\boldsymbol{r}) = m^{0}(\omega)\,\mathrm{I}^{*}(\Delta_1,\omega)\,\mathrm{I}(\Delta_2,\omega)\,, \tag{C.9}$$

$$\begin{aligned}\mathcal{C}^{\gamma}(\mathbf{1},\mathbf{2},\omega;\boldsymbol{r}) &= m^{0}(\omega)\,\hat{\boldsymbol{\Delta}}_1\cdot\hat{\boldsymbol{\Delta}}_2\\ &\quad\times\left[\mathrm{II}(\Delta_1,\omega)\,\mathrm{III}(\Delta_2,\omega)+\mathrm{II}(\Delta_2,\omega)\,\mathrm{III}^{*}(\Delta_1,\omega)\right].\end{aligned} \tag{C.10}$$

The integrals I, II, and III are given by

$$\mathrm{I}(d,\omega) = (2\pi)^3\int_0^\infty k\mathrm{d}k\; J_0(kd)\mathcal{G}^{\mathbf{\Pi}}(k,\omega)\,, \tag{C.11}$$

$$\mathrm{II}(d,\omega) = (2\pi)^6\,\Gamma^{0}(\omega)\int_0^\infty k\mathrm{d}k\; J_1(kd)G^{\mathbf{\Pi}}(k,\omega)\mathcal{G}^{\mathbf{\Pi}*}(k,\omega)\,, \tag{C.12}$$

$$\mathrm{III}(d,\omega) = (2\pi)^3\int_0^\infty \mathrm{d}k\; J_1(kd)\mathcal{G}^{\mathbf{\Pi}}(k,\omega)\,. \tag{C.13}$$

The kernels for source strength and damping are then obtained from

$$K_{\pm}^{a,\gamma}(\mathbf{1},\mathbf{2},\boldsymbol{r}) = 4\pi\mathrm{Re}\int_0^\infty \mathrm{d}\omega\; W_{\pm}^{*}(\mathbf{1},\mathbf{2},\omega)\mathcal{C}^{a,\gamma}(\mathbf{1},\mathbf{2},\omega;\boldsymbol{r}) \tag{C.14}$$

with $W_{\pm}^{*}(\mathbf{1},\mathbf{2},\omega)$ given equation 3.66. The kernels, in terms of the integrals I, II, and III, are reported in the main body of the text (eqs. [3.78] and [3.80]).

Appendix D

Single-Source Kernels for the Damping Rate

In the single-source picture, we seek an expression for the kernel $K_+^{\gamma,\mathrm{ss}}$ which provides an integral relationship between the one-way travel time $\delta\tau_+^{\mathrm{ss}}$ (eq. [3.84]) and the local damping perturbation $\delta\gamma(\boldsymbol{r})/\gamma$, i.e.

$$\delta\tau_+^{\mathrm{ss}}(\mathbf{1},\mathbf{2}) = \int_{(A)} \mathrm{d}\boldsymbol{r}\ \frac{\delta\gamma(\boldsymbol{r})}{\gamma}\ K_+^{\gamma,\mathrm{ss}}(\mathbf{1},\mathbf{2};\boldsymbol{r})\,. \tag{D.1}$$

We first rewrite the single-source definition of travel time (eq. [3.84]) in terms of the temporal Fourier transform of the signal observed at point $\mathbf{2}$:

$$\delta\tau_+^{\mathrm{ss}}(\mathbf{1},\mathbf{2}) = -\frac{\mathrm{Re}\int_0^\infty \mathrm{d}\omega\ \mathrm{i}\omega\, \phi^{0*}(\mathbf{2},\omega)\,\delta\phi(\mathbf{2},\omega)}{\int_0^\infty \mathrm{d}\omega\ \omega^2\,|\phi^0(\mathbf{2},\omega)|^2}\,. \tag{D.2}$$

Given the pressure source $\rho\Theta$, located at point $\mathbf{1}$, and defined by equation (3.85), the zero- and first-order signals observed at $\mathbf{2}$ are

$$\phi^0(\mathbf{2},\omega) = (2\pi)^4 \int_0^\infty k\mathrm{d}k\ J_0(k\Delta)\mathcal{G}^{\Pi}(k,\omega)\Theta(k,\omega)\,, \tag{D.3}$$

$$\begin{aligned}\delta\phi(\mathbf{2},\omega) &= (2\pi)^4\,\Gamma^0(\omega)\int_{(A)} \mathrm{d}\boldsymbol{r}\ \frac{\delta\gamma(\boldsymbol{r})}{\gamma}\int \mathrm{d}\boldsymbol{k}\,\mathrm{d}\boldsymbol{k}'\ e^{\mathrm{i}\boldsymbol{k}\cdot\boldsymbol{\Delta}_1-\mathrm{i}\boldsymbol{k}'\cdot\boldsymbol{\Delta}_2}\\ &\quad\times G^{\Pi}(\boldsymbol{k},\omega)\Theta(\boldsymbol{k},\omega)\ \hat{\boldsymbol{k}}\cdot\hat{\boldsymbol{k}}'\ \mathcal{G}^{\Pi}(\boldsymbol{k}',\omega)/k'\,. \end{aligned}\tag{D.4}$$

Using equation (D.2) we obtain the damping kernel $K_+^{\gamma,\mathrm{ss}}$ in the form

$$K_+^{\gamma,\mathrm{ss}}(\mathbf{1},\mathbf{2};\boldsymbol{r}) = \frac{\int_0^\infty \mathrm{d}\omega\ \omega^2|\phi^0(\mathbf{2},\omega)|^2\ \mathcal{K}_+^{\gamma,\mathrm{ss}}(\mathbf{1},\mathbf{2};\boldsymbol{r};\omega)}{\int_0^\infty \mathrm{d}\omega\ \omega^2|\phi^0(\mathbf{2},\omega)|^2}\,, \tag{D.5}$$

with the function $\mathcal{K}_+^{\gamma,\mathrm{ss}}$ (single-frequency kernel) defined by

$$\mathcal{K}_+^{\gamma,\mathrm{ss}}(\mathbf{1},\mathbf{2};\boldsymbol{r};\omega) = \hat{\boldsymbol{\Delta}}_1\cdot\hat{\boldsymbol{\Delta}}_2\ \mathrm{Im}\left[\frac{\mathbb{IV}(\Delta_1,\omega)\ \mathbb{III}(\Delta_2,\omega)}{\omega\ \phi^0(\mathbf{2},\omega)}\right]. \tag{D.6}$$

In the above equation, the function $\mathbb{IV}$ is a one-dimensional integral given by

$$\mathbb{IV}(d,\omega) = (2\pi)^3\,\Gamma^0(\omega)\int_0^\infty k\mathrm{d}k\ J_1(kd)G^{\Pi}(k,\omega)\Theta(k,\omega)\,, \tag{D.7}$$

and the function $\mathbb{III}$ denotes the integral already defined by equation (C.13). Notice from equation (D.5) that the kernel $K_+^{\gamma,\mathrm{ss}}$ is a frequency average of $\mathcal{K}_+^{\gamma,\mathrm{ss}}$ weighted by $\omega^2|\phi^0(\mathbf{2},\omega)|^2$.

In order to compute the kernel we have to make a choice for the source spectrum, $\Theta(k,\omega)$. In general, this is difficult without a priori knowledge of the zero-order cross-correlation. When comparing the definition of travel time of Appendix A with the single-source definition (eq. [3.84]), we find that a good match between the two definitions is obtained when $\phi^0(\mathbf{2},t)$ looks like $\mathrm{Hea}(t)C^0(\mathbf{1},\mathbf{2},t)$. This condition is best met when

$$\Theta(k,\omega) = -\frac{k\,F(k,\omega)\,m^0(k,\omega)}{2\Gamma^0(\omega)}\,. \tag{D.8}$$

Note that the filter function $F(k,\omega)$ appears in equation (D.8). The kernel $K_+^{\gamma,\mathrm{ss}}$, shown in Figure 3.8, was computed using this choice.

Appendix E

Constraints on Oblique Rotation of the Solar Core

The axis of rotation of the Sun's surface is inclined from the normal to the ecliptic by $7^\circ.25$. Is that true also of the rotation of the rest of the Sun? Knowledge of the direction of the angular momentum is pertinent to studies of the formation of the solar system. Moreover, Bai & Sturrock (1993) have recently interpreted temporal variations in the spatial distribution of solar flares as the outcome of the interaction of the Sun's envelope with an obliquely rotating core. We report here an attempt to determine the principal seismic axes of oscillation of the dipole and quadrupole p modes from LOI data obtained as a component of the VIRGO investigation on the spacecraft SOHO. We find that formally their most likely orientation is somewhat closer to being normal to the ecliptic than is the axis of the surface rotation. However, the uncertainty in the determination well encompasses the possibility of them being parallel to the surface rotation axis, yet it does not reject (at a level marginally greater than one standard deviation) the possibility that the Sun's angular momentum is parallel to that of the rest of the solar system.

Rotation splits the degeneracy of oscillation modes in a multiplet (having like radial order n and degree l). If angular velocity is constant on spheres, a scalar p-mode eigenfunction is approximately proportional to $\Re[Y_l^m(\theta,\phi)\exp(-\mathrm{i}\omega_m t)]$ with respect to spherical polar coordinates (r, θ, ϕ) about an appropriate axis $\mathbf{P}$. The index m denotes the azimuthal order, and Y_l^m is a spherical harmonic function. If rotation is about a unique axis **R**, then **P** coincides with **R**. But if **R** varies with r, **P** is a vector average of $\mathbf{R}(r)$, weighted with the rotational splitting kernel K of the mode (Gough & Kosovichev, 1993). When the magnitude Ω of the angular velocity varies with latitude (defined relative to $\mathbf{R}(r)$), K depends on m and, except in the case $l = 1$, the pulsation axis of the multiplet is not well defined. In the case of the Sun, the latitudinal variation of Ω is small: in the data analysis of quadrupole modes we report below, we assume that there exists a frame in which each azimuthal component can still be described geometrically in terms of a single spherical harmonic, and that the m dependence of the splitting is negligible. If the oscillation axis **P** is not coincident with the surface rotation axis **S** with respect to which one imagines solar oscillations are analysed, each harmonic projection $(l,\, m')$ with respect to **S** is actually a linear combination of normal modes, and will exhibit all the rotationally split frequencies ω_m (where m is the true azimuthal order, with respect to **P**). The orientation of **P** cannot be determined from frequencies alone, however – the frequencies of an (aspherical) object are independent of the direction from which that object is viewed. To determine **P** it is necessary to measure the eigenfunctions. A first attempt at that (Gough et al., 1995), made by estimating in the IPHIR data the amplitudes of whole-disc projections of blended components of $l = 1$ multiplets, suggested that **P** might be closer to the normal **n** to the ecliptic than is **S**, but the significance of the measurement is difficult to assess. Here we report a more sophisticated analysis of modes with $l = 1$ and $l = 2$ observed with the LOI (Appourchaux et al., 1997).

The LOI measures radiant intensity $s_p(t)$ integrated over a set of 12 pixels p. The nominal attitude of SOHO is such that the projection of **S** onto the detector should coincide with a principal axis of symmetry **d** of the detector at all times. A multiplet $(l,\, n)$ is presumed to be composed of $2l{+}1$ independently randomly excited modes m, each producing a disturbance of the form $x_m(\theta,\phi,t) \equiv f_m(t;\omega_m)Y_l^m(\theta,\phi)$ about a pulsation axis **P**. We denote by $\beta_d(t)$ the inclination of the axis **P** with respect to **d**, and by $\alpha_d(t)$ the azimuth of **P** relative to the line of sight. During the short selected interval of observation, the variation of $\alpha_d(t)$ and $\beta_d(t)$ is small, and accordingly we ignore it, replacing $\alpha_d(t)$ and $\beta_d(t)$ by their averages $\overline{\alpha}_d$ and $\overline{\beta}_d$. This approximation implies that we neglect the hyperfine structure that results

mode set	$\overline{\alpha}_d$	$\overline{\beta}_d$
$l = 1$ and $15 \le n \le 24$	$5° \pm 10°$	$4°.9 \pm 2°.5$
$l = 2$ and $14 \le n \le 24$	$10° \pm 10°$	$5°.7 \pm 1°.6$
all	$8° \pm 7°$	$5°.5 \pm 1°.4$

Table E.1: Euler angles $\overline{\alpha}_d$ and $\overline{\beta}_d$ which define the directions of the pulsation axes **P** with respect to **d**.

from SOHO's orbit about **n** (see Goode & Thompson, 1992). The sensitivity of a pixel p to a mode m can thus be expressed in terms of the Euler angles $\overline{\alpha}_d$ and $\overline{\beta}_d$ by integrating over the pixel the Fourier amplitude $\hat{x}_m(\theta, \phi, \omega)$ of x_m weighted with the limb-darkening function. Now consider a small frequency range, and construct $2l+1$ linear combinations $\hat{y}_M(\omega)$, $-l \le M \le l$, of the 12 Fourier transforms $\hat{s}_p(\omega)$ in order to isolate each component m. Using a maximum likelihood technique, we fit a parametric model to the $2l+1$ complex spectra $\hat{y}_M(\omega)$. For each discrete frequency ω, $\hat{f}_m(\omega; \omega_m)$ is presumed to be (a realization of) a centred complex Gaussian random variable whose variance is Lorentzian with amplitude A_m, linewidth Γ, and central frequency $\omega_0 + m\, a_1$, where a_1 is the mean rotational splitting. The $\hat{f}_m$ are assumed to be independent random variables. We add independent Gaussian noise to each pixel with location-dependent variance depending on three undetermined parameters N_j. The parameters ($\overline{\alpha}_d$, $\overline{\beta}_d$, ω_0, a_1, Γ, A_m, N_j) are chosen such that they maximize the joint probability density function over some frequency interval (frequency bins are assumed to be independent of each other). Realistic Monte Carlo simulations have been performed which demonstrate that the estimators are essentially unbiased.

Observations were taken over the four-month interval 1996, July 10 – Nov. 6, centred about Sept. 8 when the inclination $B_0(t)$ of **S** from the axis **d** was the greatest (on average, $\overline{B}_0 = 6°.06$). During this interval the average position of **n** is coincident with **d**. The angles $\overline{\alpha}_d$ and $\overline{\beta}_d$ where determined for each multiplet separately. Means and standard deviations are listed in Table E. From the knowledge of the satellite's orbit it is also possible to deduce constraints on the fixed azimuth α and inclination β of **P** with respect to the ecliptic normal **n** (Fig. E.1). The results are not inconsistent with **P** being coincident with **S**.

We adopt a simple two-zone model. The outer zone, $r_c < r \le R_\odot$ is assumed to

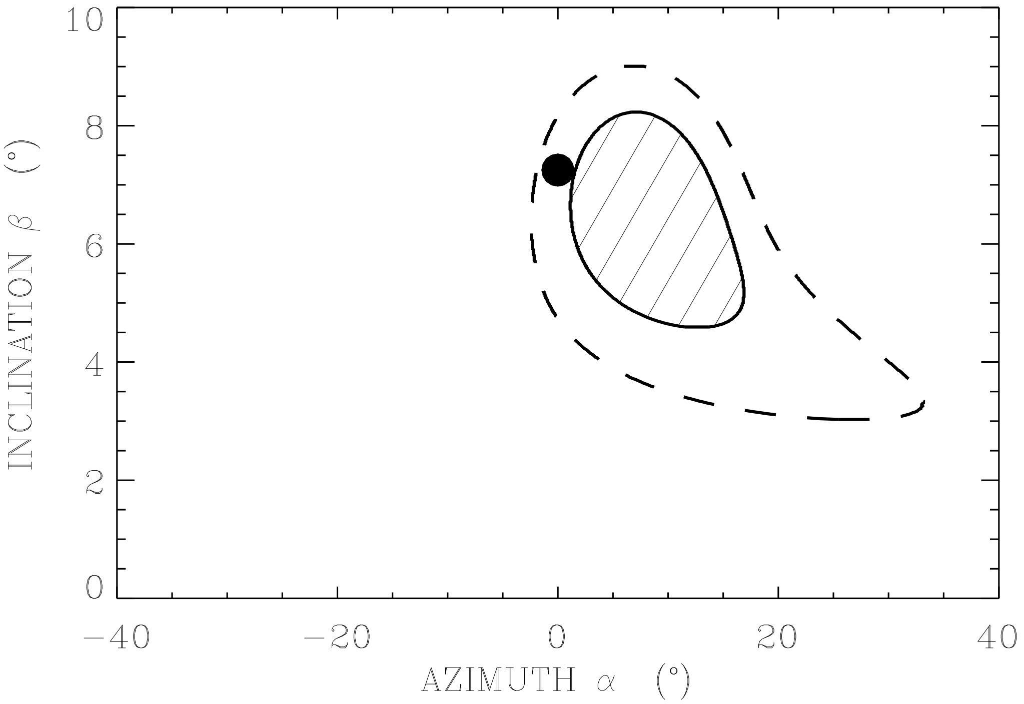

Figure E.1: Permitted orientations (α, β) of the mean pulsation axis **P** with respect to the normal **n** to the ecliptic. The hatched area and the dashed boundary refer to the 1-σ and 1.5-σ confidence levels respectively, computed under the assumption that the uncertainties in $\overline{\alpha}_d$ and $\overline{\beta}_d$ are independent. The filled circle indicates the direction of **S**.

rotate about **S** with angular velocity determined from higher-degree modes (Kosovichev et al., 1997); beneath the convection zone a uniform rate of 435 nHz was adopted. The inner zone, $0 \leq r \leq r_c$, was assumed to rotate uniformly with angular velocity Ω_c about an axis **C**. The constraints on (α, β) can then be used to constrain the obliquity β_c of **C** with respect to **S** for each value of r_c. In this way one can test, for example, the model of Bai & Sturrock (1993) in which the core rotates at a rate $\Omega_c/2\pi = 454$ nHz inclined by $\beta_c = 40°$. In this model, we find that the core radius r_c has to be less than $0.24R_\odot$ in order to be consistent with LOI data.

Subject to the same two-zone model, we can also constrain the orientation (α_L, β_L) of the axis **L** of the Sun's angular momentum with respect to the normal **n**. In Figure E.2, the hatched region in the (β_c, β_L) plane is the permitted region if α, β and a_1 are all within one standard deviation of their seismically determined values. We measured the averaged rotational splitting over the same set of modes to be $a_1 = 440 \pm 7$ nHz from one year of data. It is evident that at a level of significance

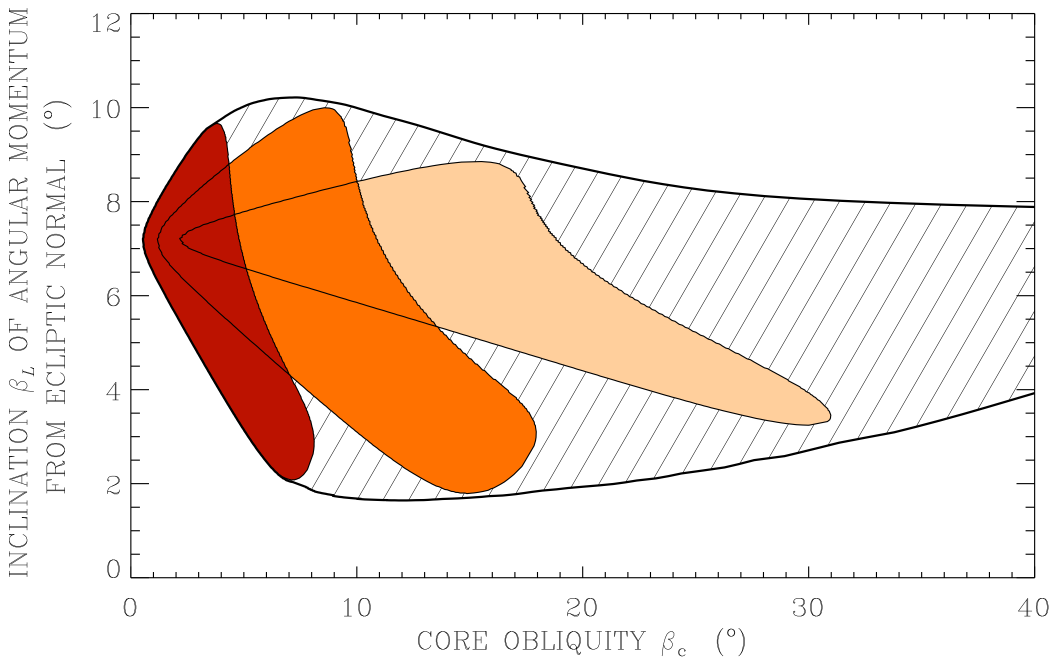

Figure E.2: Permitted inclinations β_L of the solar angular momentum when $a_1 = 440$ nHz, for $r_c/R_\odot = 0.25$ (light orange), 0.4 (orange) and 0.7 (red). The hatched area is the permitted region for $r_c < 0.7R_\odot$ and 433 nHz $< a_1 <$ 447 nHz.

only slightly above one standard deviation the possibility of **L** being perpendicular to the plane of the ecliptic is not ruled out.

Bibliography

Anderson, E. R., Duvall, T. L., & Jefferies, S. M. 1990, Astrophys. J., 364, 699

Antia, H. M., Basu, S., Hill, F., Howe, R., Komm, R. W., & Schou, J. 2001, MNRAS, 327, 1029

Appourchaux, T. 2002, private communication

Appourchaux, T., Andersen, B., Frohlich, C., Jimenez, A., Telljohann, U., & Wehrli, C. 1997, Solar Phys., 170, 27

Appourchaux, T., Chang, H.-Y., Gough, D. O., & Sekii, T. 2000, MNRAS, 319, 365

Appourchaux, T., Gizon, L., & Rabello-Soares, M.-C. 1998, Astron. Astrophys. Suppl., 132, 107

Baglin, A., Auvergne, M., Catala, C., Michel, E., & COROT Team. 2001, Proc. SOHO 10: Helio- and asteroseismology at the dawn of the millennium, Edited by A. Wilson, ESA SP-464, Noordwijk: ESA, 395

Bai, T., & Sturrock, P. A. 1993, Astrophys. J., 409, 476

Beck, J. G. 1997, PhD thesis, Univ. California at Los Angeles

Beck, J. G. 2000, Solar Phys., 191, 47

Beck, J. G., & Duvall, T. L. 2001, Proc. SOHO 10: Helio- and asteroseismology at the dawn of the millennium, Edited by A. Wilson, ESA SP-464, Noordwijk: ESA, 577

Beck, J. G., Duvall, T. L., & Scherrer, P. H. 1998, Nature, 394, 653

Beck, J. G., Gizon, L., & Duvall, T. L. 2002, Astrophys. J., 575, L47

Beck, J. G., & Schou, J. 2000, Solar Phys., 193, 333

Bedding, T. R., Butler, R. P., McCarthy, C., Kjeldsen, H., Marcy, G. W., O'Toole, S. J., Tinney, C. G., & Wright, J. 2002, Asteroseismology Across the HR Diagram. Edited by M. Thompson, M. Cunha and M. Monteiro (Kluwer)

Berrilli, F., Ermolli, I., Florio, A., & Pietropaolo, E. 1999, Astron. Astrophys., 344, 965

Birch, A. C. 2002, PhD thesis, Stanford University

Birch, A. C., & Kosovichev, A. G. 2000, Solar Phys., 192, 193

Birch, A. C., Kosovichev, A. G., Price, G. H., & Schlottmann, R. B. 2001, Astrophys. J., 561, L229

Bogdan, T. J. 1997, Astrophys. J., 477, 475

—. 2000, Solar Phys., 192, 373

Bogdan, T. J., Braun, D. C., & & Lites, B. W. 1998, Astrophys. J., 492, 379

Bogdan, T. J., M., B. T., Lites, B. W., & Thomas, J. H. 1993, Astrophys. J., 406, 723

Bouchy, F., & Carrier, F. 2001, Astron. Astrophys., 374, L5

Brandenburg, A., & Schmitt, D. 1998, Astron. Astrophys., 338, L55

Braun, D. C., Duvall, Jr., T. L., & LaBonte, B. J. 1988, Astrophys. J., 335, 1015

Braun, D. C., & Lindsey, C. 2003, Proc. SOHO 12, ESA SP-517, 15

Brown, T. M., Charbonneau, D., Gilliland, R. L., Noyes, R. W., & Burrows, A. 2001, Astrophys. J., 552, 699

Brown, T. M., & Gilliland, R. L. 1994, Ann. Rev. Astron. Astrophys., 32, 37

Brummell, N. H., Hurlburt, N. E., & Toomre, J. 1996, Astrophys. J., 473, 494

Cally, P. S., & Bogdan, T. J. 1997, Astrophys. J., 486, L67

Charbonneau, D., Brown, T. M., Latham, D. W., & Mayor, M. 2000, Astrophys. J., 529, L45

Chou, D. 2000, Solar Phys., 192, 241

Chou, D., & Dai, D. 2001, Astrophys. J., 559, L175

Chou, D.-Y., Labonte, B. J., Braun, D. C., & Duvall, T. L. 1991, Astrophys. J., 372, 314

Christensen-Dalsgaard, J., Proffitt, C. R., & Thompson, M. J. 1993, Astrophys. J., 403, L75

Corbard, T., & Thompson, M. J. 2002, Solar Phys., 205, 211

Dahlen, F. A., & Tromp, J. 1998, Theoretical Global Seismology (Princeton: Princeton Univ. Press)

DeRosa, M. L. 2001, PhD thesis, Univ. Colorado at Boulder

DeRosa, M. L., Duvall, Jr., T. L., & Toomre, J. 2000, Solar Phys., 192, 351

Deubner, F.-L. 1975, Astron. Astrophys., 44, 371

Dreizler, S., Hauschildt, P. H., Kley, W., Rauch, T., Schuh, S. L., Werner, K., & Wolff, B. 2003, Astron. Astrophys., in press

D'Silva, S., Duvall, T. L., Jefferies, S. M., & Harvey, J. W. 1996, Astrophys. J., 471, 1030

Duvall, T. L. 1979, Solar Phys., 63, 3

—. 1980, Solar Phys., 66, 213

Duvall, T. L. 1995, in ASP Conf. Ser. 76: GONG 1994. Helio- and Astro-Seismology from the Earth and Space, 465

Duvall, T. L. 1998, in Structure and Dynamics of the Interior of the Sun and Sun-like Stars SOHO 6/GONG 98 Workshop, Vol. 2, p. 581

Duvall, T. L., D'Silva, S., Jefferies, S. M., Harvey, J. W., & Schou, J. 1996, Nature, 379, 235

Duvall, T. L., & Gizon, L. 2000, Solar Phys., 192, 177

Duvall, T. L., & Harvey, J. W. 1986, NATO ASI Series C: Mathematical and Physical Sciences, Vol. 169, Seismology of the Sun and the Distant Stars, ed. D. O. Gough (Dordrecht: Reidel), 105

Duvall, T. L., Jefferies, S. M., Harvey, J. W., Osaki, Y., & Pomerantz, M. A. 1993a, Astrophys. J., 410, 829

Duvall, T. L., Jefferies, S. M., Harvey, J. W., & Pomerantz, M. A. 1993b, Nature, 362, 430

Duvall, T. L., Kosovichev, A. G., & Murawski, K. 1998, Astrophys. J., 505, L55

Duvall, T. L., Kosovichev, A. G., Scherrer, P. H., Bogart, R. S., Bush, R. I., de Forest, C., Hoeksema, J. T., Schou, J., Saba, J. L. R., Tarbell, T. D., Title, A. M., Wolfson, C. J., & Milford, P. N. 1997, Solar Phys., 170, 63

Dziembowski, W. 1977, Acta Astronomica, 27, 203

Dziembowski, W. A., & Goode, P. R. 1992, Astrophys. J., 394, 670

Favata, F., Roxburgh, I., & Christensen-Dalsgaard, J. 2000, in The Third MONS Workshop: Science Preparation and Target Selection, 49

Foglizzo, T., Garcia, R. A., Boumier, P., Charra, J., Gabriel, A. H., Grec, G., Robillot, J. M., Roca Cortes, T., Turck-Chieze, S., & Ulrich, R. K. 1998, Astron. Astrophys., 330, 341

Fossat, E. 1981, in NATO ASIC Proc. 68: Solar Phenomena in Stars and Stellar Systems, 75

Foukal, P. 1972, Astrophys. J., 173, 439

Frohlich, C., Andersen, B., Appourchaux, T., Berthomieu, G., Crommelynck, D. A., Domingo, V., Fichot, A., Finsterle, W., Gomez, M. F., Gough, D., Jimenez, A., Leifsen, T., Lombaerts, M., Pap, J. M., Provost, J., Cortes, T. R., Romero, J., Roth, H., Sekii, T., Telljohann, U., Toutain, T., & Wehrli, C. 1997, Solar Phys., 170, 1

Galloway, D. J., Proctor, M. R. E., & Weiss, N. O. 1977, Nature, 266, 686

Galloway, D. J., & Weiss, N. O. 1981, Astrophys. J., 243, 945

Giles, P. M. 2000, PhD thesis, Stanford University

Giles, P. M., Duvall, Jr., T. L., Scherrer, P. H., & Bogart, R. S. 1997, Nature, 390, 52

Giovanelli, R. G. 1980, Solar Phys., 67, 211

Gizon, L. 1998, in IAU Symp. 185, 173

Gizon, L. 2002, Astron. Nachr., 323, 251

Gizon, L., Appourchaux, T., & Gough, D. O. 1998, in IAU Symp. 185, 37

Gizon, L., & Birch, A. C. 2001, in First Solar Orbiter Workshop, ed. B. Battrick & H. Sawaya-Lacoste (Noordwijk: ESA SP-493), 233

Gizon, L., & Birch, A. C. 2002, Astrophys. J., 571, 966

Gizon, L., Birch, A. C., Bush, R. I., Duvall, T. L., Kosovichev, A. G., Scherrer, P. H., & Zhao, J. 2001a, in First Solar Orbiter Workshop, ed. B. Battrick & H. Sawaya-Lacoste (Noordwijk: ESA SP-493), 227

Gizon, L., & Duvall, T. L. 2003, in Proc. SOHO 12, ESA SP-517, 43

Gizon, L., Duvall, T. L., & Larsen, R. M. 2000, J. Astrophys. Astron., 21, 339

Gizon, L., Duvall, T. L., & Larsen, R. M. 2001b, in IAU Symp. 203, 189

Gizon, L., Duvall, T. L., & Schou, J. 2003, Nature, 421, 43 (erratum: Nature, 421, 764)

Gizon, L., & Solanki, S. K. 2003, Astrophys. J., in press

Goode, P. R., & Thompson, M. J. 1992, Astrophys. J., 395, 307

Gough, D. O. 1993, in Les Houches Session LXVII, Astrophysical Fluid Dynamics, ed. J.-P. Zahn & J. Zinn-Justin (Amsterdam: Elsevier), 399

Gough, D. O., & Kosovichev, A. G. 1993, in ASP Conf. Ser. 40: Inside the Stars, 566

Gough, D. O., Kosovichev, A. G., & Toutain, T. 1995, in ASP Conf. Ser. 76: GONG 1994. Helio- and Astro-Seismology from the Earth and Space, 55

Gough, D. O., & Thompson, M. J. 1990, MNRAS, 242, 25

Haber, D. A., Hindman, B. W., Toomre, J., Bogart, R. S., Larsen, R. M., & Hill, F. 2002, Astrophys. J., 570, 855

Haber, D. A., Hindman, B. W., Toomre, J., Bogart, R. S., Thompson, M. J., & Hill, F. 2000, Solar Phys., 192, 335

Hagenaar, H. J., Schrijver, C. J., & Title, A. M. 1997, Astrophys. J., 481, 988

Hansen, C. J., Cox, J. P., & van Horn, H. M. 1977, Astrophys. J., 217, 151

Hart, A. B. 1954, MNRAS, 114, 17

—. 1956, MNRAS, 116, 38

Harvey, J. 1985, in Future Missions in Solar, Heliospheric and Space Plasma Physics, ed. E. Rolfe & B. Battrick (Noordwijk: ESA), 199

Hathaway, D., Gilman, P., Harvey, J. W., Hill, F., Howard, R. B., Jones, H. P., Kasher, J., Leibacher, J. B., Pintar, J., & Simon, G. W. 1996, Science, 272, 1306

Hathaway, D. H. 1982, Solar Phys., 77, 341

Hathaway, D. H. 1992, Solar Phys., 137, 15

Hathaway, D. H. 1996, Astrophys. J., 460, 1027

Hathaway, D. H., Beck, J. G., Bogart, R. S., Bachmann, K. T., Khatri, G., Petitto, J. M., Han, S., & Raymond, J. 2000, Solar Phys., 193, 299

Hathaway, D. H., Beck, J. G., Han, S., & Raymond, J. 2002, Solar Phys., 205, 25

Henry, G. W., Marcy, G. W., Butler, R. P., & Vogt, S. S. 2000, Astrophys. J., 529, L41

Hill, F. 1988, Astrophys. J., 333, 996

Hindman, B., Gizon, L., Haber, D., Duvall, T., & Toomre, J. 2003, in Proc. SOHO 12, ESA SP-517, 299

Houdek, G., Balmforth, N. J., Christensen-Dalsgaard, J., & Gough, D. O. 1999, Astron. Astrophys., 351, 582

Howard, R., & LaBonte, B. 1980, Astrophys. J., 239, L33

Howard, R. F. 1996, Ann. Rev. Astron. Astrophys., 34, 75

Howe, R., Christensen-Dalsgaard, J., Hill, F., Komm, R. W., Larsen, R. M., Schou, J., Thompson, M. J., & Toomre, J. 2000, Astrophys. J., 533, L163

Hung, S.-H., Dahlen, F. A., & Nolet, G. 2000, Geophys. J. Int., 141, 175

Hurlburt, N. E., Matthews, P. C., & Proctor, M. R. E. 1996, Astrophys. J., 457, 933

Jensen, J. M., Jacobsen, B., & Christensen-Dalsgaard, J. . 2000, Solar Phys., 192, 231

Jensen, J. M., Jacobsen, B. H., & Christensen–Dalsgaard, J. 1998, in Structure and Dynamics of the Interior of the Sun and Sun-like Stars, Vol. 2 (Noordwijk: ESA), 635

Julien, K., Legg, S., McWilliams, J., & Werne, W. 1996, J. Fluid Mech., 322, 243

Kendall, M. G., & Stuart, A. 1967, The Advanced Theory of Astrophysics: Inference and Relationship, Vol. 2, 2nd ed. (London: Butler & Tanner)

Kjeldsen, H., Arentoft, T., Bedding, T., Christensen-Dalsgaard, J., Frandsen, S., & Thompson, M. J. 1998, in Structure and Dynamics of the Interior of the Sun and Sun-like Stars SOHO 6/GONG 98 Workshop, p. 385

Kjeldsen, H., & Bedding, T. R. 1995, Astron. Astrophys., 293, 87

Kjeldsen, H., & Bedding, T. R. 1998, in The First MONS Workshop: Science with a Small Space Telescope, Eds.: H. Kjeldsen, T.R. Bedding, Aarhus Universitet, p. 1.

Komm, R. W., Howard, R. F., & Harvey, J. W. 1993a, Solar Phys., 143, 19

—. 1993b, Solar Phys., 145, 1

—. 1993c, Solar Phys., 147, 207

Konacki, M., Torres, G., Jha, S., & Sasselov, D. 2003, Nature, 421, 507

Kosovichev, A. G. 1996, Astrophys. J., 461, L55

Kosovichev, A. G., & Duvall, T. L. 1997, in ASSL Vol. 225: SCORe'96 : Solar Convection and Oscillations and their Relationship, ed. F. P. Pijpers, J. Christensen-Dalsgaard, & C. S. Rosenthal (Dordrecht: Kluwer), 241–260

Kosovichev, A. G., Duvall, T. L., Birch, A. C., Gizon, L., Scherrer, P. H., & Zhao, J. 2002, Advances in Space Research, 29, 1899

Kosovichev, A. G., Duvall, T. L. . J., & Scherrer, P. H. 2000, Solar Phys., 192, 159

Kosovichev, A. G., Schou, J., Scherrer, P. H., Bogart, R. S., Bush, R. I., Hoeksema, J. T., Aloise, J., Bacon, L., Burnette, A., de Forest, C., Giles, P. M., Leibrand, K., Nigam, R., Rubin, M., Scott, K., Williams, S. D., Basu, S., Christensen-Dalsgaard, J., Dappen, W., Rhodes, E. J., Duvall, T. L., Howe, R., Thompson, M. J., Gough, D. O., Sekii, T., Toomre, J., Tarbell, T. D., Title, A. M., Mathur, D., Morrison, M., Saba, J. L. R., Wolfson, C. J., Zayer, I., & Milford, P. N. 1997, Solar Phys., 170, 43

Kubičela, A. 1973, in Solar Activity and Related Interplanetary and Terrestrial Phenomena, ed. J. Xanthakis (Berlin: Springer-Verlag), 123

Kuhn, J. R., Armstrong, J. D., Bush, R. I., & Scherrer, P. 2000, Nature, 405, 544

Kumar, P., & Basu, S. 2000, Astrophys. J., 545, L65

LaBonte, B., & Howard, R. 1982, Solar Phys., 63, 373

Lamb, H. 1932, Hydrodynamics, 6th ed. (New York: Dover)

Ledoux, P. 1951, Astrophys. J., 114, 373

Leighton, R. B., Noyes, R. W., & Simon, G. W. 1962, Astrophys. J., 135, 474

Libbrecht, K. G., & Woodard, M. F. 1990, Nature, 345, 779

Lin, H., & Kuhn, J. R. 1992, Solar Phys., 141, 1

Lindsey, C., & Braun, D. C. 2000, Solar Phys., 192, 261

Lindsey, C., Braun, D. C., Jefferies, S. M., Woodard, M. F., Fan, Y., Gu, Y., & Redfield, S. 1996, Astrophys. J., 470, 636

Lindsey, C., Braun, D. C., Jefferies, S. M., Woodard, M. F., Fan, Y., Gu, Y., & Redfield, S. 1996, Astrophys. J., 470, 636

Lissauer, J. J. 1993, Ann. Rev. Astron. Astrophys., 31, 129

Lynden-Bell, D., & Ostriker, J. P. 1967, MNRAS, 136, 293

Marcy, G. W., & Butler, R. P. 2000, Pub. Astron. Soc. Pacific, 112, 137

Marquering, H., Dahlen, F. A., & Nolet, G. 1999, Geophys. J. Int., 137, 805

Mayor, M., & Queloz, D. 1995, Nature, 378, 355

Messiah, A. 1959, Mécanique quantique, Tome 2 (Paris: Dunod)

Meunier, N. 1999, Astrophys. J., 527, 967

Miesch, M. S., Elliott, J. R., Toomre, J., Clune, T. L., Glatzmaier, G. A., & Gilman, P. A. 2000, Astrophys. J., 532, 593

Miller, P., Foukal, P., & Keil, S. 1984, Solar Phys., 92, 33

Murawski, K., & Roberts, B. 1993, Astron. Astrophys., 272, 595

Nesme-Ribes, E., Meunier, N., & Vince, I. 1997, Astron. Astrophys., 321, 323

Nigam, R., & Kosovichev, A. G. 1999, Astrophys. J., 514, L53

November, L. J. 1989, Astrophys. J., 344, 494

Noyes, R. W., Jha, S., Korzennik, S. G., Krockenberger, M., Nisenson, P., Brown, T. M., Kennelly, E. J., & Horner, S. D. 1997, Astrophys. J., 483, L111

Parker, E. N. 1955, Astrophys. J., 122, 293

—. 1963, Astrophys. J., 138, 552

—. 1973, Astrophys. J., 186, 643

—. 1979, Astrophys. J., 230, 905

Paunzen, E., Konig, M., & Dreizler, S. 1998, Astron. Astrophys., 331, 162

Pearson, F. 1990, Map Projection: Theory and Applications (Boca Raton: CRC Press)

Pierce, K. 2000, Allen's Astrophysical Quantities, ed. A. N. Cox (4th ed.; New York: Springer-Verlag)

Ploner, S. R. O., Solanki, S. K., & Gadun, A. S. 2000, Astron. Astrophys., 356, 1050

Rüdiger, G., Brandenburg, A., & Pipin, V. V. 1999, Astronomische Nachrichten, 320, 135

Rüdiger, G., Pipin, V. V., & Belvedère, G. 2001, Solar Phys., 198, 241

Rao, C. R. 1973, Linear Statistical Inference and Its Applications (2nd ed., Wiley)

Rast, M. P. 1997, in ASSL Vol. 225: SCORe'96 : Solar Convection and Oscillations and their Relationship, 135

Rast, M. P. 2003, in Proc. SOHO 12, ESA SP-517, 163

Rice, J. B. 2002, Astron. Nachr., 323, 220-235 (2002), 323, 220

Rieutord, M., Ludwig, H.-G., Roudier, T., Nordlund, A., & Stein, R. 2001, Il Nuovo Cimento C, in press

Rieutord, M., Roudier, T., Malherbe, J. M., & Rincon, F. 2000, Astron. Astrophys., 357, 1063

Rimmele, T., & Schroeter, E. H. 1989, Astron. Astrophys., 221, 137

Rogers, E. H. 1970, Solar Phys., 13, 57

Saff, E. B., & Snider, A. D. 1993, Fundamentals of Complex Analysis for Mathematics, Science, and Engineering, 2nd ed. (Upper Saddle River: Prentice Hall), sect. 8.5, p. 423

Safronov, V. S. 1972, Evolution of the Protoplanetary Cloud and formation of the Earth and the Planets, Israel Program for Scientific Translation, Jerusalem

Saio, H. 1981, Astrophys. J., 244, 299

Sakurai, J. J. 1995, Modern Quantum Mechanics (Reading, MA: Addison-Wesley)

Scherrer, P. H., Bogart, R., Hoeksema, J. T., & Yoshimura, H. 1986, in NATO ASIC Proc. 169: Seismology of the Sun and the Distant Stars, 93

Scherrer, P. H., Bogart, R. S., Bush, R. I., Hoeksema, J. T., Kosovichev, A. G., Schou, J., Rosenberg, W., Springer, L., Tarbell, T. D., Title, A., Wolfson, C. J., Zayer, I., & The MDI Engineering Team. 1995, Solar Phys., 162, 129

Schlichenmaier, R., Jahn, K., & Schmidt, H. U. 1998, Astron. Astrophys., 337, 897

Schou, J. 1992, PhD thesis, Aarhus University

—. 1999, Astrophys. J., 523, L181

—. 2003, in Proc. SOHO 12, ESA SP-517, 381

Schou, J., & Bogart, R. S. 1998, Astrophys. J., 504, L131

Schou, J., & Buzasi, D. L. 2001, Proc. SOHO 10/GONG 2000 Workshop: Helio- and asteroseismology at the dawn of the millennium, ESA SP-464, p. 391, 464, 391

Schou, J., Christensen-Dalsgaard, J., & Thompson, M. J. 1994, Astrophys. J., 433, 389

Schrijver, C. J., Hagenaar, H. J., & Title, A. M. 1997, Astrophys. J., 475, 328

Schüssler, M. 1981, Astron. Astrophys., 94, L17

Schüssler, M., & Solanki, S. K. 1992, Astron. Astrophys., 264, L13

Shine, R. A., Simon, G. W., & Hurlburt, N. E. 2000, Solar Phys., 193, 313

Simon, G. W., & Leighton, R. B. 1964, Astrophys. J., 140, 1120

Simon, G. W., & Weiss, N. O. 1968, Z. Astrophys., 69, 435

Snodgrass, H. B. 1984, Solar Phys., 94, 13

Snodgrass, H. B., & Ulrich, R. K. 1990, Astrophys. J. Suppl., 351, 309

Solanki, S. K. 2003, Astron. Astrophys. Rev., 11, 153

Spruit, H. C. 2003, Solar Phys., 213, 1

Stein, R. F. 1967, Solar Phys., 2, 385

Stein, R. F., & Nordlund, Å. 2000, Solar Phys., 192, 91

—. 2001, Astrophys. J., 546, 585

Strous, L. H., Goode, P. R., & Rimmele, T. R. 2000, Astrophys. J., 535, 1000

Tarbell, T. D., Acton, D. S., & A., F. Z. 1997, in Adaptative Optics, Vol. 13, ed. D. Hennage (Washington, DC: OSA), 96

Tassoul, M. 1980, Astrophys. J. Supp. Ser., 43, 469

Thompson, M. J., Toomre, J., Anderson, E., Antia, H. M., Berthomieu, G., Burtonclay, D., Chitre, S. M., Christensen-Dalsgaard, J., Corbard, T., Derosa, M., Genovese, C. R., Gough, D. O., Haber, D. A., Harvey, J. W., Hill, F., Howe, R., Korzennik, S. G., Kosovichev, A. G., Leibacher, J. W., Pijpers, F. P., Provost, J., Rhodes, E. J., Schou, J., Sekii, T., Stark, P. B., & Wilson, P. 1996, Science, 272, 1300

Title, A. M., Tarbell, T. D., Topka, K. P., Ferguson, S. H., Shine, R. A., & SOUP Team. 1989, Astrophys. J., 336, 475

Toner. 2001, private communication

Tong, J., Dahlen, F. A., Nolet, G., & Marquering, H. 1998, Geophys. Res. Lett., 25, 1983

Toutain, T., & Appourchaux, T. 1994, Astron. Astrophys., 289, 649

Toutain, T., & Gouttebroze, P. 1993, Astron. Astrophys., 268, 309

Udalski, A., Zebrun, K., Szymanski, M., Kubiak, M., Soszynski, I., Szewczyk, O., Wyrzykowski, L., & Pietrzynski, G. 2002, Acta Astronomica, 52, 115

Ulrich, R. K. 1970, Astrophys. J., 162, 993

Ulrich, R. K. 1988, Solar Phys., 117, 291

Ulrich, R. K. 2001, Astrophys. J., 560, 466

Vernazza, J. E., Avrett, E. H., & Loeser, R. 1981, Astrophys. J. Suppl., 45, 635

Veronis, G. 1959, J. Fluid Mech., 5, 401

Wang, H., & Zirin, H. 1989, Solar Phys., 120, 1

Woodard, M. F. 1984, PhD thesis, Univ. California at San Diego

—. 1997, Astrophys. J., 485, 890

Woodard, M. F., & Noyes, R. W. 1985, Nature, 318, 449

Worden, S. P., & Simon, G. W. 1976, Solar Phys., 46, 73

Yaglom, A. M. 1962, An Introduction to the Theory of Stationary Random Functions (Englewood Cliffs: Prentice Hall)

Yoshimura, H. 1971, Solar Phys., 18, 417

Zhao, J. 2003, in Proc. SOHO 12, ESA SP-517, 417

Zhao, J., Kosovichev, A. G., & Duvall, T. L. 2001, Astrophys. J., 557, 384

Zhao, L., & Jordan, T. H. 1998, Geophys. J. Int., 133, 683